

Article

# The Impact of the Vanadium Oxide Addition on the Physicochemical Performance Stability and Intercalation of Lithium Ions of the TiO<sub>2</sub>-rGO-electrode in Lithium Ion Batteries

Beata Kurc <sup>1,\*</sup> , Marcin Wysokowski <sup>2</sup> , Łukasz Rymaniak <sup>3</sup>, Piotr Lijewski <sup>3</sup>, Adam Piasecki <sup>4</sup>  and Paweł Fuć <sup>3</sup>

<sup>1</sup> Institute of Chemistry and Electrochemistry, Faculty of Chemical Technology, Poznan University of Technology, Berdychowo 4, PL-60965 Poznan, Poland

<sup>2</sup> Institute of Chemical Technology and Engineering, Faculty of Chemical Technology, Poznan University of Technology, Berdychowo 4, PL-60965 Poznan, Poland; marcin.wysokowski@put.poznan.pl

<sup>3</sup> Institute of Combustion Engines and Transport, Faculty of Transport Engineering, Poznan University of Technology, Piotrowo 3, PL-60965 Poznan, Poland; lukasz.rymaniak@put.poznan.pl (Ł.R.); piotr.lijewski@put.poznan.pl (P.L.); pawel.fuc@put.poznan.pl (P.F.)

<sup>4</sup> Faculty of Mechanical Engineering and Management, Institute of Materials Science and Engineering, Poznan University of Technology, Jana Pawla II 24, PL-60965 Poznan, Poland; adam.piasecki@put.poznan.pl

\* Correspondence: beata.kurc@put.poznan.pl; Tel.: +4861-665-3666

Received: 22 January 2020; Accepted: 21 February 2020; Published: 24 February 2020



**Abstract:** This work determines the effect of the addition of various amounts of vanadium oxide on the work of a cell built from a hybrid V<sub>x</sub>O<sub>y</sub>-TiO<sub>2</sub>-rGO system in a lithium-ion cell. Moreover, a new method based on solvothermal chemistry is proposed for the creation of a new type of composite material combining reduced graphene, vanadium oxide and crystalline anatase. The satisfactory electrochemical properties of V<sub>x</sub>O<sub>y</sub>-TiO<sub>2</sub>-rGO hybrids can be attributed to the perfect matching of the morphology and structure of V<sub>x</sub>O<sub>y</sub>-TiO<sub>2</sub> and rGO. In addition, it is also responsible for the partial transfer of electrons from rGO to V<sub>x</sub>O<sub>y</sub>-TiO<sub>2</sub>, which increases the synergistic interaction of the V<sub>x</sub>O<sub>y</sub>-TiO<sub>2</sub>-rGO hybrid to the reversible storage of lithium. In addition a full cell was created LiFePO<sub>4</sub>/V<sub>x</sub>O<sub>y</sub>-TiO<sub>2</sub>-rGO. The cell showed good cyclability while providing a capacity of 120 mAh g<sup>-1</sup>.

**Keywords:** solvothermal synthesis; reduced graphene oxide; anatase; vanadium oxide; lithium ion batteries

## 1. Introduction

Continuous technological progress means that people are constantly looking for new solutions that will enable them to work more efficiently and make the most of their potential. The constant movement and very active lifestyle of millions of people from around the world forces somehow being in constant motion, which makes them portable devices. Lithium-ion cells are widely used in modern technologies as separate systems.

The automotive industry continues working to introduce and promote energy saving and environmentally friendly solutions. The use of alternative fuels, hybrid and electric drives, as well as fuel cells, could be included among those [1–4]. This requires introducing significant changes in vehicle construction and even infrastructure adaptation, e.g., building battery charging stations.

Electric and hybrid drives used in city buses are characterized by many favorable operational parameters in urban operating conditions and it is in this vehicle group that ongoing efforts are being

undertaken to introduce various types of innovations to improve the efficiency of electrical solutions, mainly the energy storage systems. Their addition to hybrid systems makes it possible to turn off the internal combustion engine during stops and to use only the electric drive, e.g., in zero emission zones [5]. In this type of systems, energy is recovered when the vehicle brakes, converting the kinetic energy of the vehicle into electricity.

The search for suitable cathodic and anodic materials is still underway. Among the former there are, among others, vanadium oxides. Due to the preservation of good properties during loading and unloading processes, relatively easy transfer of lithium ions, several degrees of oxidation ( $V^{3+}$ ,  $V^{4+}$ ,  $V^{5+}$ ), ease of synthesis and lack of toxicity, they are a good basis for working with lithium-ion cells. They also provide good cycling stability [6–9]. Vanadium oxides are regularly used in research works around the world. New synthetic methods are still being developed that use this compound in the most diverse fields of science. During the preparation of the research material, various compilations using vanadium oxide are used. Such materials can be prepared by various methods including hydrothermal synthesis, precipitation [10] and sol gel synthesis [11]. In one of the recent works of Ceder et al. [12] the slow diffusion kinetics in  $V_2O_5$  electrodes was also indicated, particularly in the stable  $\alpha$ - $V_2O_5$  phase associated with the conversion during the discharge process of fully demagnesiated  $\alpha$ - $V_2O_5$  into a coexisting two-phase structure with fully magnesiated  $\alpha$ - $V_2O_5$  and fully demagnesiated  $\alpha$ - $V_2O_5$  phases. The relatively large theoretical capacity when intercalating two lithium  $Li^+$  ions per unit cell is the main advantage of this oxide.

On top of this the addition of porous  $V_2O_5$  was shown to provide interconnected network for efficient transport of  $Li^+$  across the entire structure. Moreover, the interconnected network infuses higher mechanical robustness in order to cope with the active materials volume expansion while also retaining dimensional stability at the electrode level. The feasibility of this approach has been successfully demonstrated, but the  $V_2O_5$  electrodes can from the material's poor structural stability, low-diffusion coefficient of lithium ions ( $\sim 10^{-12} \text{ cm}^2 \text{ s}^{-1}$ ) and moderate electronic conductivity ( $10^{-2}$  to  $10^{-3} \text{ S cm}^{-1}$ ) when used in rechargeable Li-ion batteries.

The unique structure could provide numerous electrolyte access channels to facilitate rapid diffusion of lithium ions into the electrode material. It also affected the short semiconductor diffusion for lithium due to the thin layer of  $V_xO_y$ . It also influenced the high electricity conductivity of the entire electrode based on the graphene network and the highest content of electrochemically active material in the electrode. The hybrid obtained using this method can meet all kinetic requirements for efficient charging and discharging of the ideal electrode material-i.e., rapid ion diffusion. As a result, the graphene structure and  $V_xO_y$  enable the electrode to work efficiently: charging and discharging with a long life cycle while maintaining a highly reversible capacity. The addition of vanadium oxide reduces structural changes during work, prevents, among others material swelling.

The following table shows sample combinations of reagents used in vanadium oxide methods as an electrode material. Depending on the purpose of the test material being prepared, different compilations of used substances are selected. The review of these substances aims to show how many possibilities exist for the use of vanadium oxide in a wide variety of lithium-ion cell research. The most common combinations with its use: rGO- $V_2O_5$ ;  $TiO_2$ - $V_2O_5$ .

rGO is widely used as a template for solvothermal deposition of  $V_2O_5$  [13] as well as  $TiO_2$  [14,15]. Surprisingly, there are no reports to date concerning the use of rGO as a template for the development of vanadia–titania nanocomposites for Li-ion batteries.

The unique structure could provide numerous electrolyte access channels to facilitate rapid diffusion of lithium ions into the electrode material. It also affected the short semiconductor diffusion for lithium due to the thin layer of  $V_xO_y$ . It also influenced the high electricity conductivity of the entire electrode based on the graphene network and the highest content of electrochemically active material in the electrode. The hybrid obtained using this method can meet all kinetic requirements for efficient charging and discharging of the ideal electrode material-i.e., rapid ion diffusion. As a result, the graphene structure and  $V_xO_y$  enable the electrode to work efficiently: charging and discharging

with a long life cycle while maintaining a highly reversible capacity. The addition of vanadium oxide reduces structural changes during work, prevents, among others material swelling.

Therefore, we decided to develop, for the first time, a solvothermal reaction for the synthesis of novel  $V_xO_y$ -TiO<sub>2</sub>-rGO nanocomposites and to investigate their potential application in the construction of a new generation of Li-ion batteries. Incorporation of rGO into  $V_xO_y$ -TiO<sub>2</sub> is beneficial in terms of the cell stability. The cell does not lose significant capacity during extended work.

## 2. Materials and Methods

### 2.1. Synthesis of $V_xO_y$ -TiO<sub>2</sub>-rGO Oxide Nanocomposites

For the typical synthesis of  $V_xO_y$ -TiO<sub>2</sub>-rGO oxide nanocomposites, a solution consisting of 20 mL of H<sub>2</sub>O and 40 mL of CH<sub>3</sub>COOH (Sigma-Aldrich, Hamburg, Germany) underwent vigorous stirring at room temperature; then 2 mL of rGO (Merck, Hamburg, Germany), 10 mL of titanium(IV) butoxide (Sigma-Aldrich), an appropriate quantity of NH<sub>4</sub>VO<sub>3</sub> (Merck) and 1 mL of NH<sub>4</sub>OH (Merck) were added gradually. The detailed quantities of reagents used for the synthesis of selected samples are given in Table 1, Figure 1.

**Table 1.** Description of the reactants and conditions used for solvothermal synthesis of  $V_xO_y$ -TiO<sub>2</sub>-rGO composites.

Sample Name	Volume of H <sub>2</sub> O/mL	CH <sub>3</sub> COOH/mL	Amount of NH <sub>4</sub> VO <sub>3</sub> /g	Volume of Ti(OC <sub>4</sub> H <sub>7</sub> ) <sub>4</sub> /mL	Temperature/K	Time/h
S <sub>2</sub> V <sub>0</sub> Ti <sub>1</sub>	20	40	0	10	473	24
S <sub>2</sub> V <sub>0.25</sub> Ti <sub>1</sub>			0.1			
S <sub>2</sub> V <sub>0.5</sub> Ti <sub>1</sub>			0.2			
S <sub>2</sub> V <sub>1</sub> Ti <sub>1</sub>			0.4			

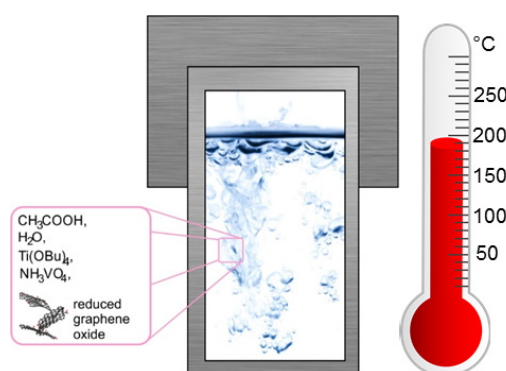


**Figure 1.** Schematic view of the solvothermal synthesis procedure.

### 2.2. Electrode and Electrolyte

The tested anodes were analyzed:  $V_xO_y$ -TiO<sub>2</sub>-rGO on a copper foil (Hohsen, city, Japan)|LiPF<sub>6</sub> solid salt in liquid EC/DMC (1:1)|Li. The ratio of components was  $V_xO_y$ -TiO<sub>2</sub>-rGO (75%), AB (15%), PVdF (10%), (by weight). In order to get rid of the NMP solvent, the electrodes were dried under vacuum for 24 h at 120 °C.

### 2.3. Procedures and Measurements

The morphology and microstructure of the prepared samples were examined on the basis of the SEM images recorded from an EVO40 scanning electron microscope (Zeiss, Oberkochen, Germany). The particle size distributions were determined using a Zetasizer Nano ZS (Malvern Instruments Ltd.).

A Vertex 70 spectrophotometer (Bruker, Bremen, Germany) was used to record the Fourier transform infrared spectra (FTIR). Analysis was conducted on the materials in the form of tablets, with the WAXS method used for crystal phase identification analysis. The results were analyzed using X-RAYAN software. To determine the electrochemical properties of the cells electrochemical impedance spectroscopy (EIS) and galvanostatic charging/discharging tests were used. The cycling measurements were taken using a Gammry Industries (Louis Drive Warminster, PA 18974) multichannel electrochemical system at different current density values, while the multichannel potentiostat (Gammry) was used for cyclic voltammetry (CV).

In order to assess the morphologies of particles, the scanning electron microscope (SEM), model MIRA3, produced by Tescan (Brno–Kohoutovice, Czech Republic) was used. An accelerating voltage of 20 kV was applied. The chemical compositions of powders were measured by ULTIM MAX 65 microanalyzer with EDS method (Oxford Instruments) at the same accelerating voltage i.e., 20 kV. The contents of elements such as Ti, O and V were analyzed. To reduce samples charging, the graphite film with thickness of about 20 nm was coated on powders using a JEE 4B vacuum evaporator (JEOL, Dearborn Road Peabody, MA, USA).

The electrodes: Li: ca. 45 mg ( $0.785 \text{ cm}^2$ ),  $\text{V}_x\text{O}_y\text{-TiO}_2\text{-rGO}$ : 2.5–3.5 mg, were separated by a glass microfiber GF/A separator (Whatmann, 0.4–0.6 mm thick). The electrodes were placed in an adapted Swagelok<sup>®</sup> connecting tube. Cells were assembled in a glove box in a dry argon atmosphere.

### 3. Results

#### 3.1. Dispersive and Structural Properties of the Obtained Materials

The SEM images presented below indicate that  $\text{TiO}_2\text{-rGO}$  ( $\text{S}_2\text{V}_0\text{Ti}_1$ ) obtained by a solvothermal method without the presence of vanadium precursor has a uniform spherical shape with particle sizes ranging between 50 nm and 150 nm, and a tendency to form aggregates. This observation was confirmed by measurements of particle size distribution (Figure 2).

The graph obtained confirms a bimodal particle size distribution resulting from the aggregation of nanoparticles into sub-micrometric aggregates. The SEM images and the particle size distribution graphs presented for samples obtained with increasing quantities of vanadium precursor show an increasing tendency towards the formation of large conglomerates composed of spherical nanoparticles (Figure 2).

To confirm composite formation and to identify the functional groups present on the surface of the obtained materials, FTIR spectroscopy was applied. Figure 3a shows the spectra recorded for  $\text{V}_x\text{O}_y\text{-TiO}_2\text{-rGO}$  composite samples and for  $\text{TiO}_2\text{-rGO}$  as a reference sample. The fundamental vibrations in all of the  $\text{TiO}_2$ -based composites appear in the FTIR spectra as a very intense broad band, ascribed to stretching vibrations of Ti–O bonds ( $550\text{--}653 \text{ cm}^{-1}$ ) [16,17]. The next band is visible at  $1103 \text{ cm}^{-1}$ , and according to the literature [18] is related to stretching vibrations of unshared V=O bonds [19]. The highest intensity of this band is observed for the sample obtained with the highest quantity of vanadium precursor. The band visible at  $1333 \text{ cm}^{-1}$  is a result of stretching vibrations of C=O and C–OH bonds. The multiple bands visible in a range from  $1414 \text{ cm}^{-1}$  to  $1551 \text{ cm}^{-1}$  are related to the graphitic core of reduced graphene oxide [20,21]. The intense band at  $\sim 1630 \text{ cm}^{-1}$  corresponds to deformation vibrations of adsorbed water molecules [16], but also overlaps with a band related to C=C  $\text{sp}^2$  bonded carbon atoms [22,23]. The intense wide band at  $3407 \text{ cm}^{-1}$ , with a shoulder at  $3241 \text{ cm}^{-1}$ , is attributed to stretching vibrations of O–H groups [16].

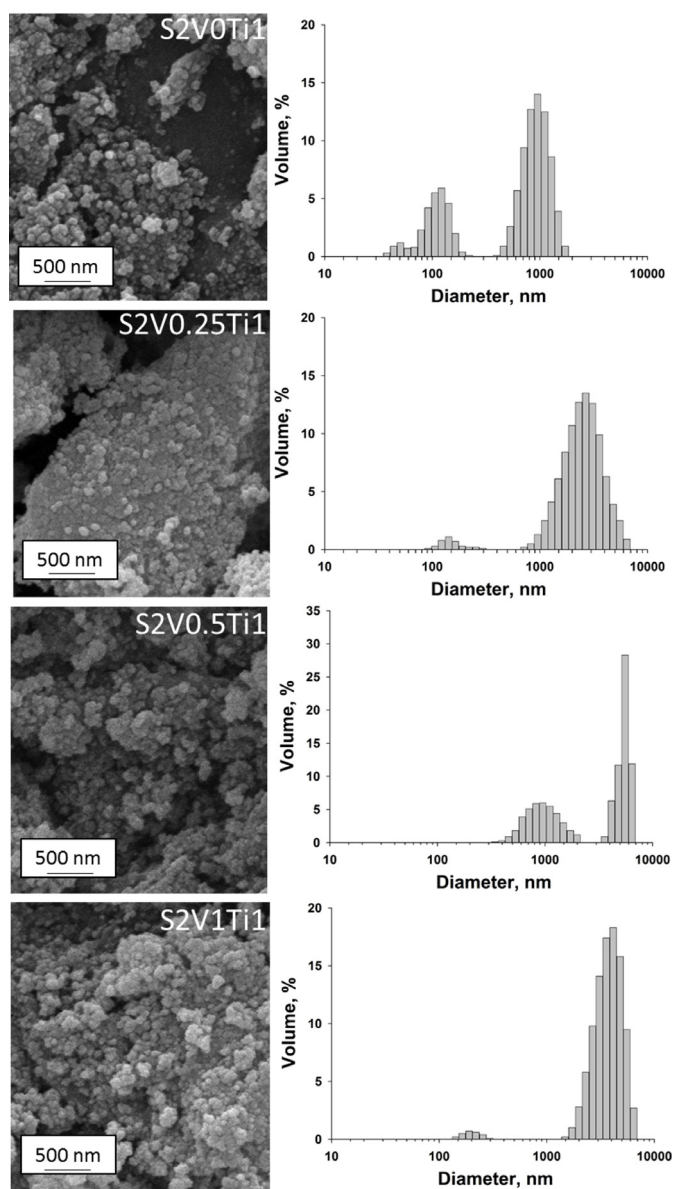


Figure 2. SEM micrographs and particle size distributions of the obtained materials.

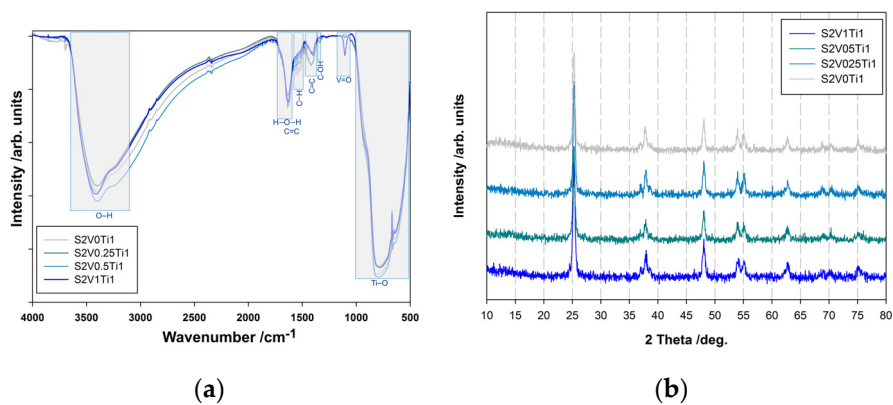


Figure 3. (a) FTIR spectra of the obtained materials; (b) XRD patterns of the prepared composites.

The XRD patterns of the samples are presented in Figure 3b. All patterns confirm that the materials synthesized via the solvothermal method exhibit very high crystallinity. All observed  $2\theta$  peaks are

characteristic for anatase (JCPDS, No. 21–1272). It can be observed that the incorporation of vanadium precursor does not lead to the formation of any new crystalline phase, and does not influence the crystallinity of the obtained materials.

Nevertheless, the fact that no vanadium phases (such as the  $V_2O_5$  orthorhombic phase) are observed in these XRD measurements indicates that the vanadium oxide is deposited as an amorphous coating on the  $TiO_2$  nanoparticles.

In Figure 4 the results of chemical composition studies were presented as the EDS spectrums. In the tables, the concentrations of the studied elements (Ti, O and V) as well as the standard deviation were presented. The studies from the area of  $1\text{ mm}^2$  were carried out.

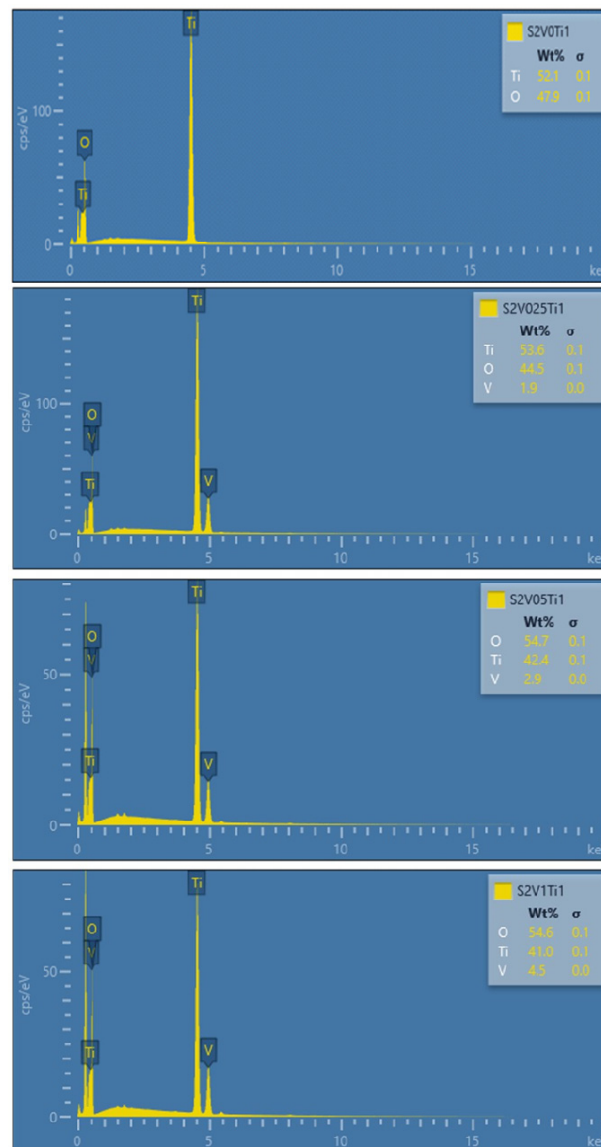
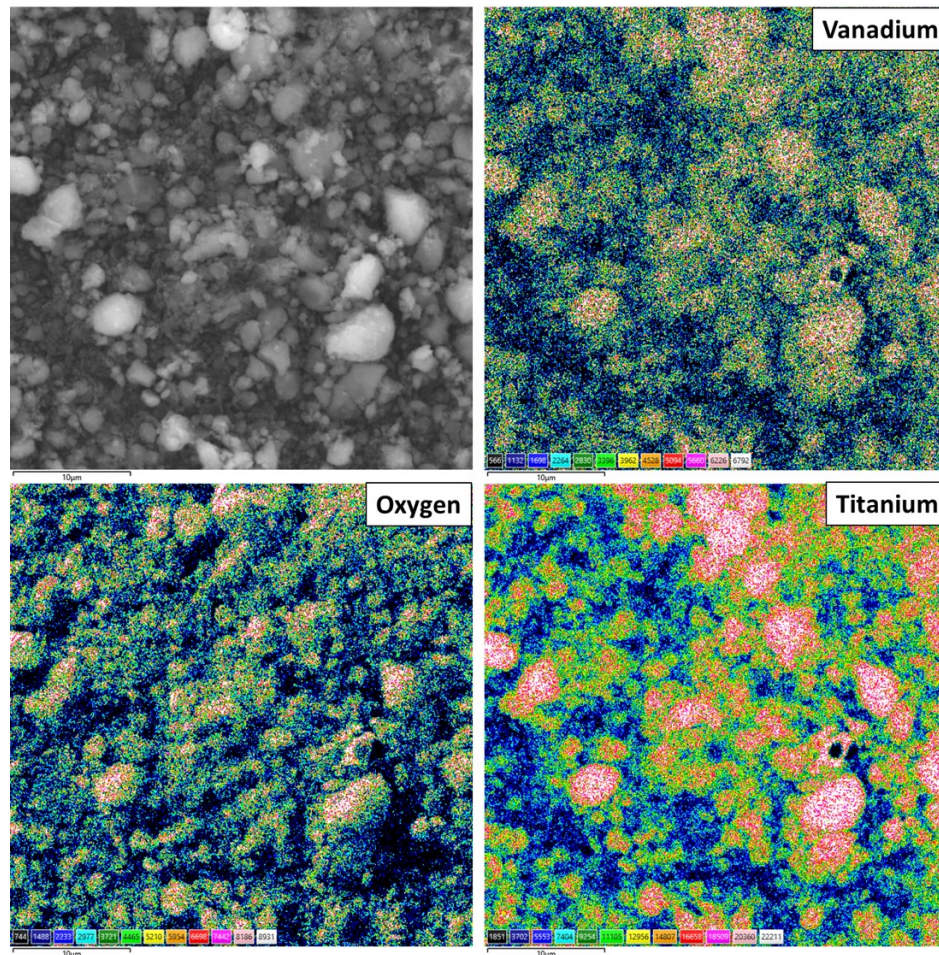


Figure 4. EDS spectra of the obtained materials.

The  $S_2V_0Ti_1$  sample was characterized by the highest content of titanium and oxygen, whereas for the  $S_2V_1Ti_1$  sample the highest content of vanadium, i.e., 4.5 wt% was measured.

In Figure 5 SEM image and EDS concentration maps of V, O and Ti for the sample  $S_2V_1Ti_1$  were presented. The maps are shown using a 12 color scale. The colors corresponded to the concentration of a selected element, the white pixels meant the highest concentration of element and the black areas corresponded to a concentration equal to zero. The numerical values corresponded to the number of

counts. After applying individual areas on each other, it could be stated that areas with light and dark colors overlapped. Thus, the resulting material in the form of a powder with particle sizes from 0.4 to 5  $\mu\text{m}$  was homogeneous in respect of chemical composition. The intensity was compatible to the results presented in the form of EDS spectrums in Figure 4.



**Figure 5.** SEM image and EDS concentration maps of V, O and Ti for the sample  $\text{S}_2\text{V}_1\text{Ti}_1$ .

### 3.2. Electrochemical Properties

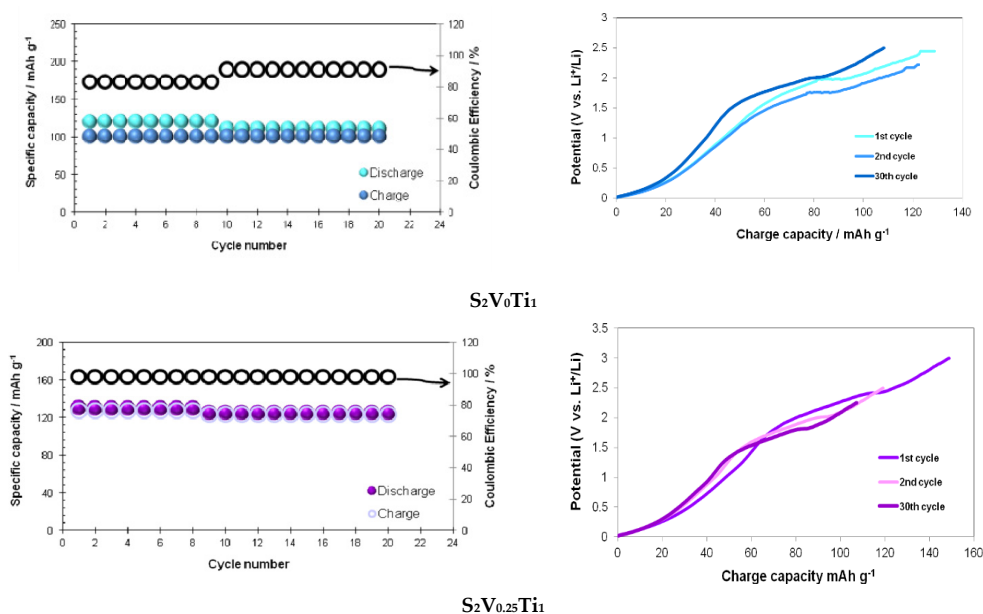
Nanoscience and nanotechnology offers some new perspectives. Novel techniques and increased understanding of material science have made it possible to create and craft appropriate anode materials for new LIBs. Thanks to the appropriate physicochemical characteristics of the structures, lithium storage has been achieved. In addition, a high lithium-ion flux at the electrode/electrolyte interface has been obtained, the diffusion distance for both Li and electron ions has been reduced, and anode volume changes during the charging/discharging process have been significantly reduced. By combining all of the aforementioned features into new devices it should be possible to create new high energy density and high power density devices.

The  $\text{V}_x\text{O}_y\text{-TiO}_2\text{-rGO}$  composite anode exhibited stable cycle performance, while retaining a discharge capacity of  $160 \text{ mAh g}^{-1}$  after the 50th cycle. This is comparable to the capacities reported in the literature [24–36] (see Table 2).

**Table 2.** Comparison of the type of materials (various  $V_xO_y$ ) with preparation methods in the literature.

Reference	Electrode Materials	Discharge Capacity/mAh $g^{-1}$	Current/mA $g^{-1}$
[15]	Carbon-coated $Li_3VO_4$ ( $Li_3VO_4/C$ )	370	15C (C = 394)
[24]	$Li_xV_2O_5$	116	C/4 (C = 294)
[25]	$Li_3VO_4$ /graphene nanosheets composite ( $Li_3VO_4$ /graphene)	223	20C (C = 400)
[26]	$V_2O_5$	273	0.2C (C = 294)
[26]	$V_2O_5$ -300	256	0.2C (C = 300)
[26]	$V_2O_5$ -400	210	0.2C (C = 300)
[26]	$V_2O_5$ -400	195	0.2C (C = 300)
[27]	$LiNi_{0.5}Co_{0.2}Mn_{0.3}O_2$ was surface-modified by double-layer coating: $V_2O_5$ , graphene oxide (GO-VO-NCM)	125	0.2C (C = 270)
[27]	VO-NCM	130	0.2C (C = 270)
[28]	$Li_3VO_4/C$ -Ni composite	325	10C (C = 180)
[29]	$LiV_2O_5$	135	C/5 (C=294)
[6]	rGO- $V_2O_5$	295	10C (C = 394)
[31]	$TiO_2$ - $V_2O_5$	319	100
[32]	Hierarchical $V_2O_5$ nanobelts ( $V_2O_5$ -HNbs)	248	50
[33]	$V_2O_5$ - $TiO_2$	452	50
[34]	$TiO_2$ - $V_2O_5$	195	17
[35]	Ag- $TiO_2/V_2O_5$	300	50
[36]	$Li_3VO_4/C$	360	100

The results of the cyclability study of all investigated materials are presented in Figure 6. The cycling behavior of the  $V_xO_y$ - $TiO_2$ -rGO electrode is plotted at a low current density of  $50 \text{ mA } g^{-1}$ , as shown in Figure 5.  $S_2V_0Ti_1$  exhibit the initial discharge–charge capacities of 110 and 120  $\text{mAh } g^{-1}$ , respectively. In the first cycle, a relatively high specific capacity was observed, which is a common phenomenon. In the literature, this is translated as the formation of solid electrolyte interphase (SEI). When cycling to the 30th cycle, the capacity is  $100 \text{ mAh } g^{-1}$  and then it gradually increases to  $85 \text{ mAh } g^{-1}$  in the  $500 \text{ mA } g^{-1}$  (Table 3).

**Figure 6.** Cont.

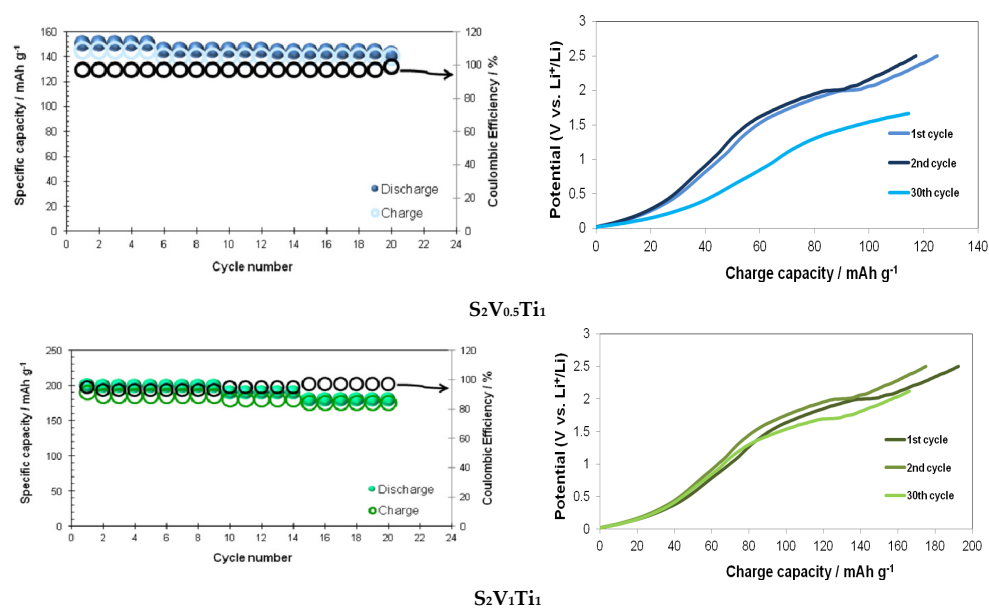


Figure 6. Galvanostatic charging and discharging with the system  $V_xO_y$ - $TiO_2$ -rGO|Li at  $50 \text{ mA g}^{-1}$ .

Table 3. Rate performance under various current densities of  $V_xO_y$ - $TiO_2$ -rGO.

Current Rate/ $\text{mA g}^{-1}$	SAMPLE NAME/CAPACITY $\text{mAh g}^{-1}$		
	$S_2V_0Ti_1$	$S_2V_{0.25}Ti_1$	$S_2V_{0.5}Ti_1$
50 (20th cycle)	120	134	155
100 (40th cycle)	110	122	143
150 (60th cycle)	100	113	134
200 (80th cycle)	90	104	121
300 (100th cycle)	90	100	120
500 (120th cycle)	85	95	118

Moreover Table 3 shows the multiple-current galvanostatic result of the  $V_xO_y$ - $TiO_2$ -rGO electrode, with discharge capacities of:  $S_2V_0Ti_1$ : 120–85  $\text{mAh g}^{-1}$ ;  $S_2V_{0.25}Ti_1$ : 134–95  $\text{mAh g}^{-1}$ ;  $S_2V_{0.5}Ti_1$ : 155–118  $\text{mAh g}^{-1}$  at current densities of 50, 100, 150, 200, 300 and 500  $\text{mA g}^{-1}$ , respectively.

Figure 6 shows charge discharge capacities depending on the number of cycles, and the profile of charging curves relative to the potential. As you can see, the most stable and simultaneously reversible arrangement turned out to be  $S_2V_1Ti_1$ . Coulombic efficiency is close to 96% and slight differences in charging curves at 1st, 2nd and 30th cycles.

The electrode material is a composite and therefore the capacities given have not been corrected for the vanadium oxide content. It was observed that, after 120 cycles ( $S_2V_{0.5}Ti_1$ ) at higher current density, the prepared material still shows an impressive discharge capacity of  $\sim 118 \text{ mAh g}^{-1}$  at a current density of 500  $\text{mA g}^{-1}$  (Table 3). All samples show relatively good capacity retention after cycles with gradually increasing currents. One may notice that  $S_2V_1Ti_1$  shows reversible capacities of about 182  $\text{mAh g}^{-1}$  at 50  $\text{mA g}^{-1}$  (Figure 6), and this value drops to 120  $\text{mAh g}^{-1}$ .

The specific capacity is low-suggesting that lithium incorporation is limited under these conditions and that surface vanadate oxides do not significantly improve ion diffusion at the electrolyte interface. To determine the performance of the  $S_2V_1Ti_1$  porous electrode in practical applications, a complete cell with a commercial LFP cathode was assembled (Figure 7).

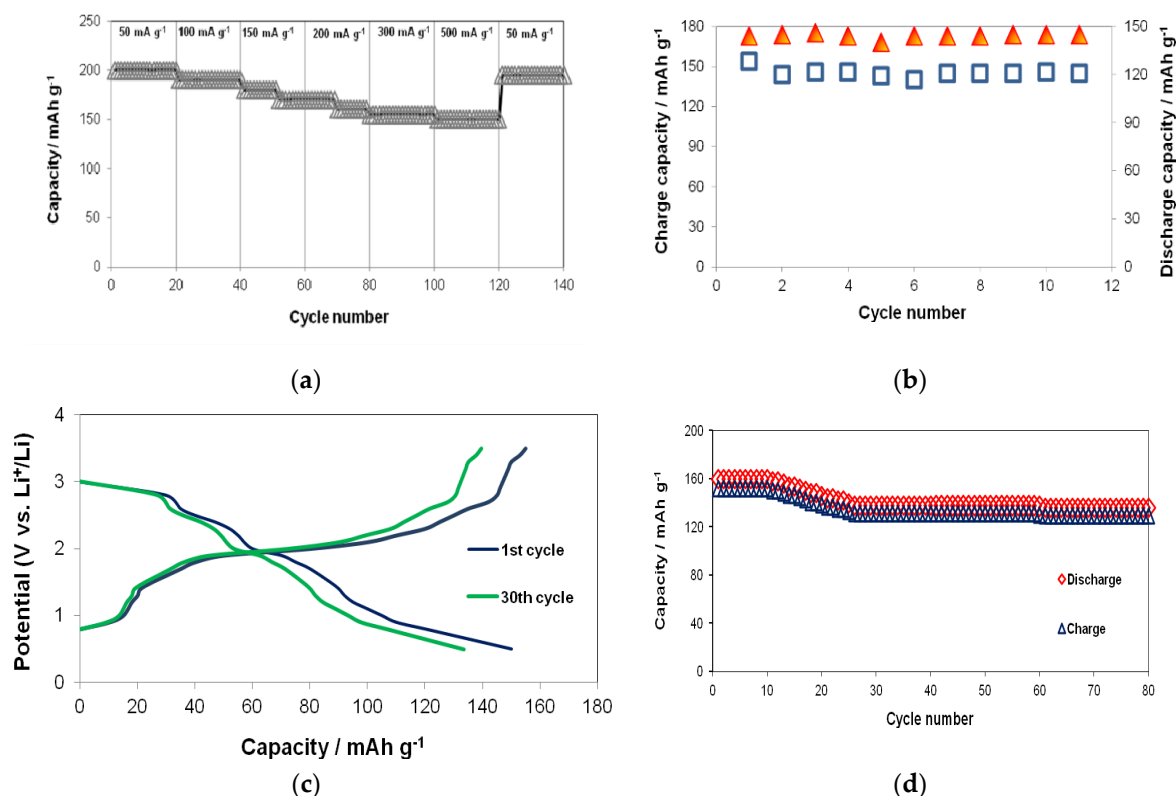


**Figure 7.** Rate performance under various current densities of  $S_2V_1Ti_1/Li$  (a); the cycling performance of the Li/LiFePO<sub>4</sub> system at C/5 (b); the charging/discharging curves of the full cell at 3C ( $S_2V_1Ti_1$  anode and LiFePO<sub>4</sub> cathode) (c); cycling performance of the full cell at 3C.

Charge/Discharge capacity of the commercial LiFePO<sub>4</sub> half cell at C/5 is shown in Figure 7a. Figure 6 shows the dependence of Li/ $S_2V_1Ti_1$  cell capacity on the cycle, taking into account the current densities at which the measurements were made. As can be seen in the chart above, the capacity decreases with subsequent cycles, especially at high current density values. Comparing the above results with literature data we get very similar values. In studies on the impact of the  $V_xO_y$  structure in lithium-ion cells, the results obtained at 50 cycles and the current of the same density oscillate in the range of 200–150 mAh g<sup>-1</sup> depending on the sample. However, in studies using reduced graphene oxide and  $V_xO_y$  in lithium-ion cells, values after 50 cycles were approximately 200 mAh g<sup>-1</sup>.

The full cell provides a discharge capacity of 158 mAh g<sup>-1</sup> in the first cycle (Figure 7c), which decreases slowly as the number of cycles increases. At a discharge capacity of 137 mAh g<sup>-1</sup> after 30 cycles. Previous studies have shown that a decrease in capacity in a full cell can be the result of many parameters, among others: different current density between two electrodes, loss of Li ions in the direction of SEI formation and other side reactions or the use of inappropriate electrolyte.

It was found that the system achieves quite good efficiency, with a return current density of up to 50 A g<sup>-1</sup>, because the discharge capacity reaches initial values (Figure 7a). When analyzing the SEI layers, it is important to remember about good synergy with the electrode material, in addition, it is important that it does not dissolve in the electrolyte (especially at high temperatures). It should be a good electronic insulator and an efficient ion conductor for lithium ions, while removing the solvation coating around lithium ions. The latter aims to avoid co-intercalation of the solvent, which is associated with the exfoliation of active material [19].

The SEI layer is formed on the electrode surface due to electrolyte decomposition (solvent and salt) at potential below 1 V vs. Li/Li<sup>+</sup> (usually 0.7 V vs. Li/Li<sup>+</sup> for most electrolytes). The potential for SEI formation, composition and stability depends on many factors, such as electrolyte formulation, charge and discharge rate, etc. [19].

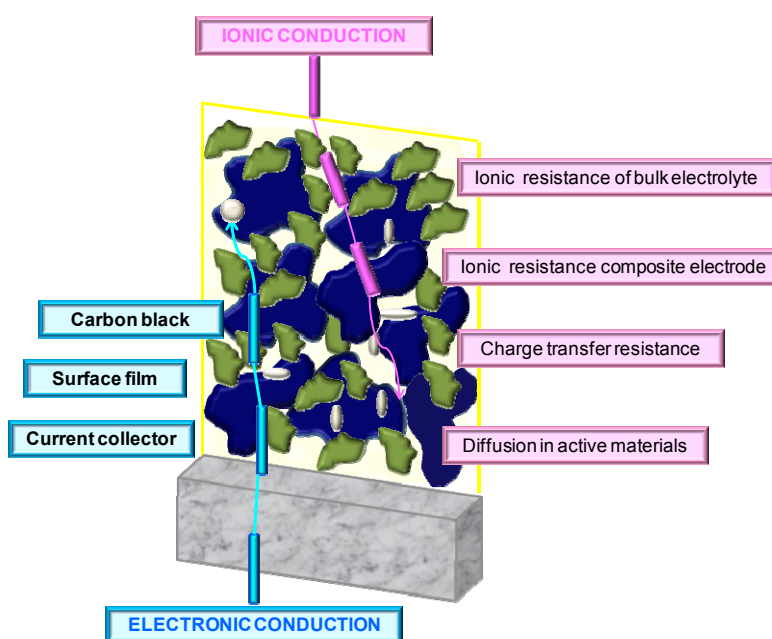
Power losses are referred to as “irreversible”. However, it is very well known that in many cases the original capabilities are “recoverable”. It has been proven that the loss of capacity results from many factors that cause the increase in SEI—this is the case with carbon anodes. The “irreversible” loss of capacity in a balanced cell is caused by the phenomenon in which the lithium involved in the reaction comes from the cathode. Similar phenomena are known when SEI is formed on the cathode and the lithium does not have enough lithium to restore the cathode to full capacity after charging [20].

The nature of the electrolyte and the composition of the solvent components have a significant impact on the nature of SEI. This is a key issue that governs the performance of both hard and soft carbon anode materials.

The prepared composite can, therefore, endure significant changes, including low or high current densities, and yet retain stability upon cycling. This is an advantage for LIBs with high power and long lifecycle as it can increase their abuse tolerance.

The storage capacity that occurs through an intercalation path, is closely associated to the surface area, morphology, crystallinity and its orientation. Soft carbons are commonly used and well accepted in the battery industry.

The presented Scheme 1 emphasizes that both the current collectors and the electrolyte side come from electrons and lithium ions in the electrodes. It was found that there are a number of resistances that are characteristic of a composite electrode, including surface resistances of so-called active materials, which are associated with conduction paths.



**Scheme 1.** Proposed of schematic illustration of composite electrode.

Ion resistance in electrolyte and solid state diffusion in active materials is directly related to ionic conductivity. For larger-size lithium-ion batteries, the distribution of reactions can occur within composite electrodes. This is most likely due to the fact that the electrode reaction occurs preferentially in areas with lower resistance. When creating composite electrodes, remember the relationship between electron/ion conductivity and the distribution of reactions in electrodes and battery performance. The distribution model has previously been studied from a theoretical point of view. There are several reports in which the distribution of composite electrode reactions is directly observed. The reactions between the electrode and the electrolyte depend on: material composition, its morphology, porosity of the composite material used for electrode construction. In addition, the morphological image determines their effective ionic and electronic conductivity.

The tuning of such composite electrodes, however, has been mostly based on the intuition and experience of the person performing it. This is because it is especially difficult to distinguish the electronic conductivity and the ionic conductivity in composite electrodes [34–37].

In addition, heterogeneous aggregation of nanostructures may affect the performance of individual cells. For longer nanostructures, the intercalation of the second lithium ion is limited, and the phase  $\delta$  completely transforms into the  $\gamma$  phase without irreversible reactions with slower kinetics, which in turn increases the structural stability of the material. In the literature, it can be argued that the electrochemical properties of nanostructures strongly depend on the particle size: the smaller the particle size, the lower the polarization and higher cell capacity.

To increase the conductivity and specific surface area of active materials, graphene and nanomaterials are used. This also causes a significant reduction in the phenomenon of agglomeration during cyclical work.

In numerous literature we already find systems containing vanadium oxides and graphene nanocomposites, such as  $V_xO_y @ G$ . The problem, however, is the controlled synthesis of vanadium oxides on graphene nanoparticles of various structures. This is an important aspect from the point of view of electrochemical properties obtained [38–43]. It is important to obtain a stable, homogeneous and composite with good structural reserve, based on  $V_2O_5$ /reduced graphene oxide.

The synergistic effect between vanadium oxide and the graphene substrate affects performance and excellent cyclic stability. This is influenced by: the growth of  $V_2O_5$  nanoparticles on reduced graphene oxide, which also ensures good electronic conductivity of electrode materials. Porous space created by interconnected nanocomponents can improve the availability of electrolyte with electrode materials. What's more, the thickness of one thin component can reduce the diffusion of  $Li^+$  ions. It also limits the transport of electrons; and the porous structure may better account for changes in volume during the cycle [44,45]. Figure 8 shows representative cyclic voltammograms (CVs) of  $S_2V_0Ti_1$ ,  $S_2V_{0.25}Ti_1$ ,  $S_2V_{0.5}Ti_1$  and  $S_2V_1Ti_1$  for the first cycles at a scan rate of  $0.5 \text{ mV s}^{-1}$  in a voltage window of 0–3 V.

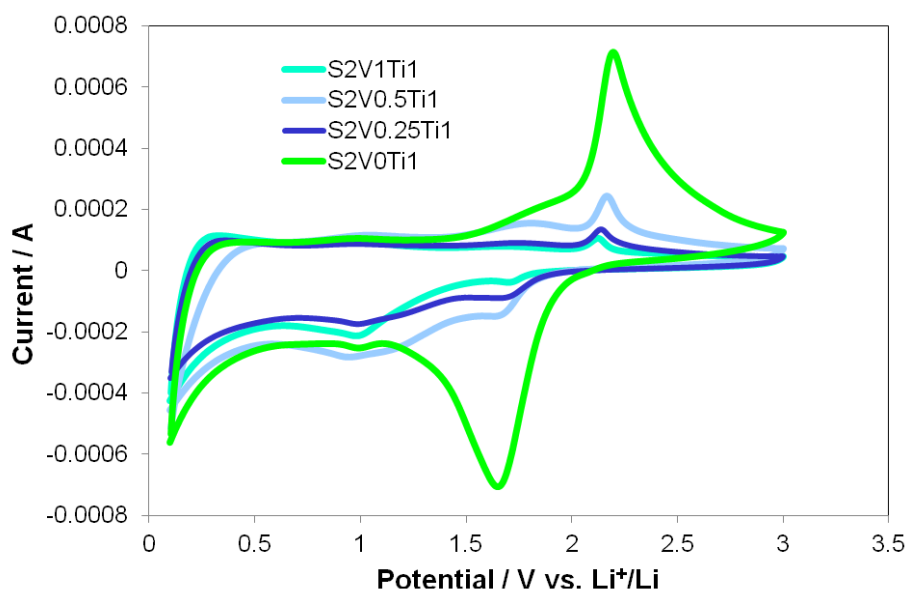


Figure 8. Cyclic voltammograms at a scan rate of  $0.5 \text{ mV s}^{-1}$ .

Cyclic voltammetry is a technique used to determine the range of potentials at which the cell will exhibit the best properties. It also provides us with information on the processes taking place on the electrodes. Figure 6 shows the cycle of the tested cell with the feed rate of  $0.5 \text{ mV s}^{-1}$ . The reduction process in cells using vanadium oxide as the electrode material is 1.6 V. The oxidation reaction corresponds to a potential of 2.25 V. In similar studies regarding modified  $V_2O_5$  used in lithium-ion

cells [46], the reduction peak appeared in the vicinity of 2.3 V. In contrast, the peak corresponding to the oxidation reactions occurred in the 2.5 V range, which is close to the above results.

As can be seen, the reduction peak shifts to the low potential region with increasing content of  $\text{TiO}_2$ , whereas the oxidation peaks shift to the high potential region, suggesting polarization under a high scan rate. The cyclic voltammograms (CVs) is widely performed to study the oxidation/reduction process and Li intercalation/deintercalation behavior in the electrode reactions.

Poor electrochemical performance can often still be caused by a minimal increase in volume as well as irreversible reactions during cyclic operation. This is also affected by the inadequate internal conductivity of  $\text{V}_2\text{O}_5$  [45–47]. Various solutions can be found in the literature: intervention in structure design or planned morphology, for example  $\text{V}_2\text{O}_5$  with a carbon coating. In the literature, we see that simple and direct strategies to solve this problem are used—the introduction of conductive carbon into the composite, physical mitigation of volume growth by creating an empty structure or exposing certain aspects by regulating morphology. Further network level design is relatively small, especially on an atomic scale, but Cao et al. [48] found that amorphous vanadium pentoxide exhibits better energy density and cycle stability than crystalline ones when used in batteries. Good properties have been shown to result from the isotropic percolated diffusion network in amorphous  $\text{V}_2\text{O}_5$ , which facilitates fast-faradic reactions. It has also been noticed that crystalline  $\text{V}_2\text{O}_5$  can provide higher capacity than amorphous  $\text{V}_2\text{O}_5$  at high current densities, while amorphous provides higher capacity at low current densities [15,49].

Figure 9 shows scanning electron microscopy (SEM) images of pristine electrodes and after electrochemical cycling. The  $\text{S}_2\text{V}_0\text{Ti}_1$  and  $\text{S}_2\text{V}_1\text{Ti}_1$  particles after electrochemical cycling are covered with a film and small aggregates. This ‘micro-roughness’ may indicate the formation of an SEI layer.

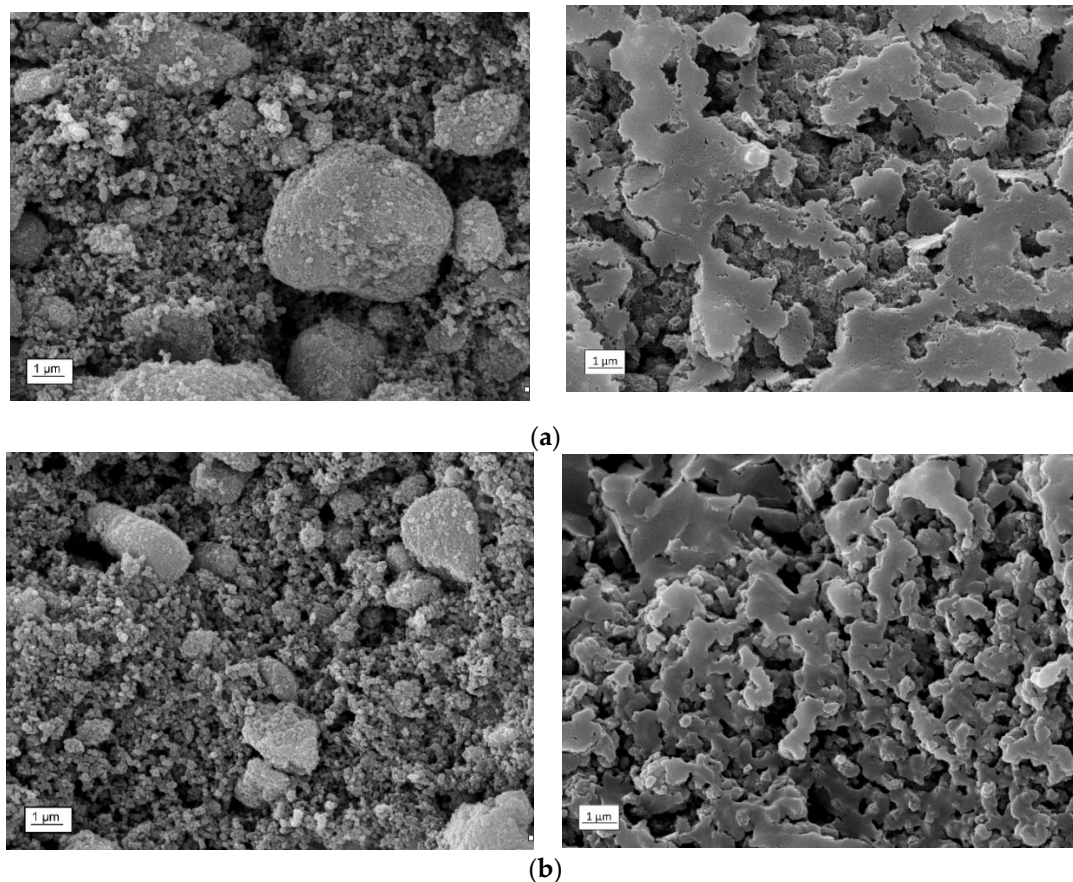


**Figure 9.** SEM images of obtained materials: (a)  $\text{S}_2\text{V}_0\text{Ti}_1$ ; (b)  $\text{S}_2\text{V}_1\text{Ti}_1$ . (left) Before charging/discharging; (right) After charging/discharging.

Robust intercalation tunnels and the ability of many electrons to pass, produces a  $V_2O_5$  electrode with high power efficiency, which requires the use of dimensional parameters and transport to overcome the complex environment of physicochemical reactions. Likely by the directions of ion diffusion towards the electrode and load transfer to the electrode/electrolyte interface, which created a new aspect of research that scientists are currently trying to solve.

Using the thermodynamic expression, it should be noted that the available energy depends on the electrode materials, it is difficult to fully release the theoretical value of the chemical energy accumulated in  $V_2O_5$  due to the limitations of ion diffusion kinetics and  $V_2O_5$  computer conductivity.

#### 4. Conclusions

The solvothermal method has been shown to be an efficient tool for the preparation of  $V_xO_y$ - $TiO_2$ -rGO materials with uniform spherical morphology. The addition of vanadium precursor to the reaction system facilitates the aggregation of particles into large agglomerates. XRD measurements indicate that the vanadium atoms are well incorporated in the  $TiO_2$  crystalline structure. The work has demonstrated that  $V_xO_y$ - $TiO_2$ -rGO displays improved electrochemical stability upon the reported lithiation and delithiation, which effectively improves the long-term electrochemical performance and maintains the specific capacity well. The  $V_xO_y$ - $TiO_2$ -rGO microparticles synthesized as described here may be a promising candidate as an anode material for future application in LIBs.

It has been proved that a relatively porous structure allowed the use of the surface area to quickly replenish electrolyte ions. It has also been found that the surface porosity of various structures can create an interconnected network for better  $Li^+$  transport throughout the structure. In addition, this limited the significant increase in volume during electrode operation.

**Author Contributions:** B.K.: original draft preparation, investigation and methodology of electrochemical properties, M.W.: original draft preparation of physicochemical properties; A.P.: investigation, software, formal analysis, Ł.R.: visualization, P.L. and P.F.: project administration, funding acquisition. All authors have read and agreed to the published version of the manuscript.

**Funding:** The research was funded by European Union from European Regional Development Fund through the National Centre for Research and Development (Narodowe Centrum Badań i Rozwoju)—research project within the Operational Smart Growth Programme (contract No. POIR.01.02.00-00-0310/16-00). Application for project co-funding within Sectoral Programme INNOMOTO.

**Conflicts of Interest:** The authors declare no conflict of interest.

#### References

1. Ziolkowski, A. Automotive Thermoelectric Generator impact on the efficiency of a drive system with a combustion engine. *MATEC Web Conf.* **2017**, *118*, 00024. [[CrossRef](#)]
2. Bajerlein, M.; Rymaniak, L.; Swiatek, P.; Ziolkowski, A.; Daszkiewicz, P.; Dobrzynski, M. Modification of a Hybrid City Bus Powertrain in the Aspect of Lower Fuel Consumption and Exhaust Emissions. *Appl. Mech. Mater.* **2014**, *518*, 108–113. [[CrossRef](#)]
3. Skretowicz, M.; Sroka, Z. Analysis of application of alternative drive systems for international heavy-duty transport on Wroclaw-Dresden-Prague routes. *E3S Web Conf.* **2017**, *22*, 00159. [[CrossRef](#)]
4. Gis, W.; Merkisz, W.J. The development status of electric (BEV) and hydrogen (FCEV) passenger cars park in the world and new research possibilities of these cars in real traffic conditions. *Combust. Engines* **2019**, *178*, 144–149.
5. Ubide, D.; Larrodé, E.; de Velasco, J. New Hybrid Bus Prototype for Clean Urban Transportation. *SAE Trans.* **2003**, *6*, 704–710.
6. Pandey, G.P.; Liu, T.; Brown, E.; Yang, Y.; Li, Y.; Sun, X.S.; Fang, Y.; Li, J. Mesoporous Hybrids of Reduced Graphene Oxide and Vanadium Pentoxide for Enhanced Performance in Lithium-Ion Batteries and Electrochemical Capacitors. *Appl. Mater. Interfaces* **2016**, *8*, 9200–9210. [[CrossRef](#)] [[PubMed](#)]
7. Yang, Y.; Kim, D.; Yang, M.; Schmuki, P. Vertically aligned mixed  $V_2O_5$ - $TiO_2$  nanotube arrays for supercapacitor applications. *Chem. Comm.* **2011**, *47*, 7746–7748. [[CrossRef](#)]

8. Rakhi, R.B.; Nagaraju, D.H.; Beaujuge, P.; Alsharef, H.N. Supercapacitors based on two dimensional VO<sub>2</sub> nanosheet electrodes in organic gel electrolyte. *Electrochim. Acta* **2016**, *220*, 601–608. [[CrossRef](#)]
9. Felix-Quintero, H.; Angulo-Rocha, J.; Murrieta, S.H.; Hernandez, A.J.; Camarillo, G.E.; Flores, J.M.C.; Alejo-Armenta, C.; Garcia-Hipolito, M.; Ramos-Brito, F. Study on grow process and optical properties of ZnO microrods synthesized by hydrothermal method. *J. Luminescence* **2017**, *182*, 107–113. [[CrossRef](#)]
10. Li, H.X.; Jiao, L.F.; Yuan, H.T.; Zhao, M.; Zhang, M.; Wang, Y.M. High-performance Cu-doped vanadium oxide (Cu<sub>x</sub>V<sub>2</sub>O<sub>5</sub>) prepared by rapid precipitation method for rechargeable batteries. *Mater. Lett.* **2007**, *61*, 101–104.
11. Saravanakumar, B.; Purushothaman, K.K.; Muralidharan, G. Interconnected V<sub>2</sub>O<sub>5</sub> Nanoporous Network for High-Performance Supercapacitors. *ACS Appl. Mater. Interfaces* **2012**, *4*, 4484–4490. [[CrossRef](#)] [[PubMed](#)]
12. Gautam, G.S.; Canepa, P.; Abdellahi, A.; Urban, A.; Malik, R.; Ceder, G. The Intercalation Phase Diagram of Mg in V<sub>2</sub>O<sub>5</sub> from First-Principles. *Chem. Mater.* **2015**, *27*, 225–230. [[CrossRef](#)]
13. Foo, C.Y.; Sumboja, A.; Tan, D.J.; Wang, J.X.; Lee, P.S. Flexible and Highly Scalable V<sub>2</sub>O<sub>5</sub>-rGO Electrodes in an Organic Electrolyte for Supercapacitor Devices. *Adv. Energy. Mater.* **2014**, *4*, 1400236–1400241. [[CrossRef](#)]
14. Wang, P.; Han, L.; Zhu, C.; Zhai, Y.; Wang, S.P. Aqueous-phase synthesis of Ag-TiO<sub>2</sub>-reduced graphene oxide and Pt-TiO<sub>2</sub>-reduced graphene oxide hybrid nanostructures and their catalytic properties. *Nano Res.* **2011**, *4*, 1153–1162. [[CrossRef](#)]
15. Liang, Z.; Zhao, Y.; Dong, Y.; Kuang, Q.; Lin, X.; Liu, X.; Yan, D. The low and high temperature electrochemical performance of Li<sub>3</sub>VO<sub>4</sub>/C anode material for Li-ion batteries. *J. Electroanal. Chem.* **2015**, *745*, 1–7. [[CrossRef](#)]
16. Bezrodna, T.; Puchkovska, G.; Shymanovska, V.; Baran, H.; Ratajczak, J. IR-analysis of H-bonded H<sub>2</sub>O on the pure TiO<sub>2</sub> surface. *J. Mol. Struct.* **2004**, *700*, 175–181. [[CrossRef](#)]
17. Roşu, M.C.; Socaci, C.; Floare-Avrăm, V.; Borodi, G.; Pogăcean, F.; Coros, M.; Măgerusan, L.; Pruneanu, S. Photocatalytic performance of graphene/TiO<sub>2</sub>-Ag composites on amaranth dye degradation. *Mater. Chem. Phys.* **2016**, *179*, 232–241. [[CrossRef](#)]
18. Calvo, F.; Li, Y.; Kiawi, D.M.; Bakker, J.M.; Parneix, P.; Janssens, E. Nonlinear effects in infrared action spectroscopy of silicon and vanadium oxide clusters: Experiment and kinetic modeling. *Phys. Chem. Chem. Phys.* **2015**, *17*, 25956–25967. [[CrossRef](#)]
19. Patil, C.E.; Jadhav, P.R.; Tarwal, N.L.; Deshmukh, H.P.; Karanjkar, M.M.; Patil, P.S. Electrochromic performance of mixed V<sub>2</sub>O<sub>5</sub>-MoO<sub>3</sub> thin films synthesized by pulsed spray pyrolysis technique. *Mater. Chem. Phys.* **2011**, *126*, 711–716. [[CrossRef](#)]
20. Mutyala, S.; Mathiyarasu, J. Reagentless non-enzymatic hydrogen peroxide sensor using electrochemically reduced graphene oxide modified glassy carbon electrode. *Mater. Sci. Eng. C* **2016**, *69*, 398–406. [[CrossRef](#)]
21. Zhuo, Q.; Ma, Y.; Gao, J.; Zhang, P.; Xia, Y.; Tian, Y.; Sun, X.; Zhong, J.; Sun, X. Facile Synthesis of Graphene/Metal Nanoparticle Composites via Self-Catalysis Reduction at Room Temperature. *Inorg. Chem.* **2013**, *52*, 3141–3147. [[CrossRef](#)]
22. Verma, R.; Samdarshi, S.K.; Sagar, K.; Konwar, B.K. Nanostructured bi-phasic TiO<sub>2</sub> nanoparticles grown on reduced graphene oxide with high visible light photocatalytic detoxification. *Mater. Chem. Phys.* **2017**, *186*, 202–211. [[CrossRef](#)]
23. Wysokowski, M.; Motylenko, M.; Rafaja, D.; Koltsov, I.; Stocker, H.; Szalaty, T.J.; Bazhenov, V.V.; Stelling, A.L.; Beyer, J.; Heitmann, J.; et al. Extreme Biomimetic approach for synthesis of nanocrystalline chitin-(Ti,Zr)O<sub>2</sub> multiphase composites. *Mater. Chem. Phys.* **2017**, *188*, 115–124. [[CrossRef](#)]
24. Jung, H.; Gerasopoulos, K.; Talin, A.A.; Ghodssi, R. In situ characterization of charge rate dependent stress and structure changes in V<sub>2</sub>O<sub>5</sub> cathode prepared by atomic layer deposition. *J. Power Sources* **2017**, *340*, 89–97. [[CrossRef](#)]
25. Shi, Z.; Wang, J.Z.; Chou, S.L.; Wexler, D.; Li, H.J.; Ozawa, K.; Liu, H.K.; Wu, Y.P. Hollow Structured Li<sub>3</sub>VO<sub>4</sub> Wrapped with Graphene Nanosheets in Situ Prepared by a One-Pot Template-Free Method as an Anode for Lithium-Ion Batterie. *Nano Lett.* **2013**, *13*, 4715–4720. [[CrossRef](#)] [[PubMed](#)]
26. Zhang, X.; Wang, J.G.; Liu, H.; Liu, H.; Wei, B. Coaxial MoS<sub>2</sub>@Carbon Hybrid Fibers: A Low-Cost Anode Material for High-Performance Li-Ion Batteries. *Materials* **2017**, *10*, 250–255.
27. Luo, W.; Zheng, B. Improved electrochemical performance of LiNi<sub>0.5</sub>Co<sub>0.2</sub>Mn<sub>0.3</sub>O<sub>2</sub> cathode material by double-layer coating with graphene oxide and V<sub>2</sub>O<sub>5</sub> for lithium-ion batteries. *Appl. Surf. Sci.* **2017**, *404*, 310–317.

28. Zhang, J.; Ni, S.; Kang, T.; Tang, J.; Yang, X.; Zhang, L. Prominent electrochemical performance of a  $\text{Li}_3\text{VO}_4/\text{C}$ -Ni anode via hierarchically porous architecture design. *J. Mater. Chem. A* **2016**, *4*, 14101–14105. [[CrossRef](#)]
29. Przesniak-Welenc, M.; Karczewski, J.; Smalc-Koziorowska, J.; Łapinski, M.; Sadowska, W.; Koscielska, B. The influence of nanostructure size on  $\text{V}_2\text{O}_5$  electrochemical properties as cathode materials for lithium ion batteries. *RSC Adv.* **2016**, *6*, 55689–55694. [[CrossRef](#)]
30. Zhou, X.; He, T.; Chen, X.; Sun, L.; Liu, Z. Influence of  $\text{TiO}_2$  surface coating on the electrochemical properties of  $\text{V}_2\text{O}_5$  micro-particles as a cathode material for lithium ion batteries. *RSC Adv.* **2016**, *6*, 53925–53931. [[CrossRef](#)]
31. Niu, C.; Li, J.; Jin, H.; Shi, H.; Zhu, Y.; Wang, W.; Cao, M. Self-template processed hierarchical  $\text{V}_2\text{O}_5$  nanobelts as cathode for high performance lithium ion battery. *Electrochim. Acta* **2015**, *182*, 621–628. [[CrossRef](#)]
32. Pan, L.; Zhu, X.D.; Xie, X.M.; Liu, Y.T. Delicate ternary heterostructures achieved by hierarchical co-assembly of Ag and  $\text{Fe}_3\text{O}_4$  nanoparticles on  $\text{MoS}_2$  nanosheets: Morphological and compositional synergy in reversible lithium storage. *J. Mater. Chem. A* **2015**, *3*, 2726–2730. [[CrossRef](#)]
33. Escamilla-Perez, A.M.; Louvain, N.; Kaschowitz, M.; Freunberger, S.; Fontaine, O.; Boury, B.; Brun, N.; Mutin, P.H. Lithium insertion properties of mesoporous nanocrystalline  $\text{TiO}_2$  and  $\text{TiO}_2$ - $\text{V}_2\text{O}_5$  microspheres prepared by non-hydrolytic sol-gel. *J. Sol-Gel Sci. Technol.* **2016**, *79*, 270–278.
34. Yan, D.J.; Zhu, X.D.; Wang, K.X.; Gao, X.T.; Feng, Y.J.; Sun, K.N.; Liu, Y.T. Facile and elegant self-organization of Ag nanoparticles and  $\text{TiO}_2$  nanorods on  $\text{V}_2\text{O}_5$  nanosheets as a superior cathode material for lithium-ion batteries. *J. Mater. Chem. A* **2016**, *4*, 4900–4909. [[CrossRef](#)]
35. Hu, S.; Song, Y.; Yuan, S.; Liu, H.; Xu, Q.; Wang, Y.; Wang, C.-X.; Xia, Y.-Y. A hierarchical structure of carbon-coated  $\text{Li}_3\text{VO}_4$  nanoparticles embedded in expanded graphite for high performance lithium ion battery. *J. Power Source* **2016**, *303*, 333–339. [[CrossRef](#)]
36. Newman, J.; Tiedemann, W. Potential and Current Distribution in Electrochemical-Cells-Interpretation of the Half-Cell Voltage Measurements as a Function of Reference-Electrode Location. *J. Electrochem. Soc.* **1993**, *140*, 1961–1968. [[CrossRef](#)]
37. Ng, S.H.; La Mantia, F.; Novak, P. A Multiple Working Electrode for Electrochemical Cells: A Tool for Current Density Distribution Studies. *Angew. Chem. Int. Ed.* **2009**, *48*, 528–532. [[CrossRef](#)] [[PubMed](#)]
38. Liu, J.; Kunz, M.; Chen, K.; Tamura, N.; Richardson, T.J. Visualization of Charge Distribution in a Lithium Battery Electrode. *J. Phys. Chem. Lett.* **2010**, *1*, 2120–2123. [[CrossRef](#)]
39. Nanda, J.; Remillard, J.; O'Neill, A.; Bernardi, D.; Ro, T.; Nietering, K.E.; Go, G.-Y.; Miller, T. Local State-of-Charge Mapping of Lithium-Ion Battery Electrodes. *Adv. Funct. Mater.* **2011**, *21*, 3282–3290. [[CrossRef](#)]
40. Yoo, E.; Kim, J.; Hosono, E.; Zhou, H.-S.; Kudo, T.; Honma, I. Large reversible Li storage of graphene nanosheet families for use in rechargeable lithium ion batteries. *Nano Lett.* **2008**, *8*, 2277–2282. [[CrossRef](#)]
41. Wang, X.; Shi, G. Flexible graphene devices related to energy conversion and storage. *Energy Environ. Sci.* **2015**, *8*, 790–823. [[CrossRef](#)]
42. Gwon, H.; Kim, H.-S.; Lee, K.U.; Seo, D.-H.; Park, Y.C.; Lee, Y.-S.; Ahn, B.T.; Kang, K. Flexible energy storage devices based on graphene paper. *Energy Environ. Sci.* **2011**, *4*, 1277–1283. [[CrossRef](#)]
43. Yang, S.; Gong, Y.; Liu, Z.; Zhan, L.; Hashim, D.P.; Ma, L.; Vajtai, R.; Ajayan, P.M. Bottom-up approach toward single-crystalline  $\text{VO}_2$ -graphene ribbons as cathodes for ultrafast lithium storage. *Nano Lett.* **2013**, *13*, 1596–1601. [[CrossRef](#)] [[PubMed](#)]
44. Zhang, Y.; Pan, A.; Liang, S.; Chen, T.; Tang, Y.; Tan, X. Reduced graphene oxide modified  $\text{V}_2\text{O}_3$  with enhanced performance for lithium-ion battery. *Mater. Lett.* **2014**, *137*, 174–177. [[CrossRef](#)]
45. Xu, J.; Li, Z.; Zhang, X.; Huang, S.; Jiang, S.; Zhu, Q.; Sun, H.; Zakharova, G.S. Self-assembled  $\text{V}_3\text{O}_7$ /graphene oxide nanocomposites as cathode material for lithium-ion batteries. *Int. J. Nanotechnol.* **2014**, *11*, 808–818. [[CrossRef](#)]
46. Liu, Y.; Wang, Y.; Zhang, Y.; Liang, S.; Pan, A. Controllable Preparation of  $\text{V}_2\text{O}_5$ /Graphene Nanocomposites as Cathode Materials for Lithium-Ion Batteries. *Nanoscale Res. Lett.* **2016**, *11*, 549–553. [[CrossRef](#)] [[PubMed](#)]
47. Pan, X.; Ren, G.; Hoque, M.N.F.; Bayne, S.; Zhu, K.; Fan, Z. Fast Supercapacitors Based on Graphene-Bridged  $\text{V}_2\text{O}_3/\text{VO}_x$  Core-Shell Nanostructure Electrodes with a Power Density of  $1 \text{ MW kg}^{-1}$ . *Adv. Mater. Interfaces* **2014**, *1*, 1400398–1400406. [[CrossRef](#)]

48. Cui, C.J.; Wu, G.M.; Shen, J.; Zhou, B.; Zhang, Z.H.; Yang, H.Y.; She, S.F. Synthesis and electrochemical performance of lithium vanadium oxide nanotubes as cathodes for rechargeable lithium-ion batteries. *Electrochim. Acta* **2010**, *55*, 2536–2541. [[CrossRef](#)]
49. Su, D.W.; Dou, S.X.; Wang, G.X. Hierarchical orthorhombic V<sub>2</sub>O<sub>5</sub> hollow nanospheres as high performance cathode materials for sodium-ion batteries. *J. Mater. Chem.* **2014**, *2*, 11185–11194. [[CrossRef](#)]



© 2020 by the authors. Licensee MDPI, Basel, Switzerland. This article is an open access article distributed under the terms and conditions of the Creative Commons Attribution (CC BY) license (<http://creativecommons.org/licenses/by/4.0/>).